Density Functional Theory-Based Molecular Dynamics Simulation of Acid-Catalyzed Chemical Reactions in Liquid Trioxane

Alessandro Curioni,*,†,‡ Michiel Sprik,† Wanda Andreoni,† Heinz Schiffer,§ Jürg Hutter,†,|| and Michele Parrinello†,||

Contribution from the IBM Research Division, Zurich Research Laboratory, 8803 Rüschlikon, Switzerland, Scuola Normale Superiore, 56126 Pisa, Italy, Hoechst AG Scientific Computing, 65926 Frankfurt am Main, Germany, and Max-Planck-Institut für Festkörperforschung, 70569 Stuttgart, Germany

Received March 24, 1997[⊗]

Abstract: *Ab initio* molecular dynamics simulation is used to investigate the kinetics and thermodynamics of some of the chemical reactions that occur during the induction phase of acid-catalyzed polymerization of 1,3,5-trioxane. In particular, the first *ab initio* calculation of a free-energy profile in a condensed-phase system is presented. The introduction of an H^+ ion to a sample of trioxane liquid initiates the complete protolysis of several trioxane molecules in a rapid succession of picoseconds. Subsequently, the re-formation of small formaldehyde oligomers is observed, which break up again after 1−2 ps. The fast kinetics is found to be consistent with the results of a constrained *ab initio* molecular dynamics evaluation of the free-energy profile for the formation of a protonated dimer. In the trioxane−formaldehyde mixture, this reaction is found to be barrierless with a reaction free energy in the thermal range (10 kJ mol^{-1}). Solvation of the chemically active carbocation by formaldehyde molecules reduces the binding energy compared to that in the gas phase by 1 order of magnitude.

I. Introduction

Polymerization reactions are often initiated and propagate in or at the surface of a condensed phase. Understanding the intricacies of the reaction thermodynamics and kinetics in such a complex environment is a challenge in terms of both experiment and theory.[1] Because it involves a combination of first-principles electronic structure calculations and finite temperature dynamics, *ab initio* molecular dynamics (MD)[2] is a promising theoretical tool to help resolve and identify the many competing chemical processes that can occur in such a system. *Ab initio* MD trajectories provide us with information on the full atomic details of a chemical event (in the adiabatic limit for the electronic states). On the basis of density functional theory (DFT), the number of degrees of freedom can be extended into a range where simulation of condensed-phase systems, including liquids, becomes feasible. We have applied this method in an investigation of some of the steps involved in the formation of polyoxymethylenes (POM).

Polyoxymethylenes consist of linear chains of $-CH_2-O-$ units terminated by various types of end groups or closing on itself in a cyclic structure.[1,3−5] The simplest form of POM is paraformaldehyde, which consists of a mixture of polyoxymethylene glycols $HO-(CH_2O)_n-H$ of limited length (n = 8−100). POMs of larger lengths (n > 100) can be prepared by anionic polymerization of formaldehyde or cationic polymerization of 1,3,5-trioxane, the cyclic trimer of formaldehyde. The synthesis of high molecular weight POMs was long restricted to the laboratory, owing to thermal degradation, which starts at the hemiacetal end groups ($-CH_2-O-CH_2-OH$) and reduces a long chain to a distribution of shorter chains similar to paraformaldehyde. Application to commercial materials (acetal plastics and resins) thus had to wait until adequate stabilization methods had been developed. One of these methods is copolymerization of 1,3,5-trioxane (TXN) with a few percent of comonomer,[6] e.g., 1,3-dioxolane (DXL). Copolymerization introduces random interruption of the $-CH_2-O-$ bonds of the acetal backbone by $-CH_2-CH_2-$ units, which prevents depolymerization (unzipping). Cationic copolymerization of TXN is the basis of the Celanese−Hoechst process by which POM is produced on an industrial scale using $BF_3{\cdot}OEt_2$ as the primary catalyst.

The basic chemistry of cationic TXN polymerization is well understood and has been described in the literature.[3−7] Many open questions remain, however, and the understanding of the key steps of the polymerization process at the microscopical level is far from being complete. One serious difficulty is the inherent complexity of the process, which involves a large number of coupled chemical transformations. Simultaneously with the addition of monomers, other chemical processes take the polymers apart or rearrange them (called a chain transfer). The attack on acetal oxygen atoms by H^+ ions is an example of such a reaction that works in both directions. On the one hand, protonation of acetal oxygen atoms opens the TXN rings

* Corresponding author, present address: IBM Research Division, Zurich Research Laboratory, 8803 Rüschlikon, Switzerland.
† IBM Research Division.
‡ Scuola Normale Superiore.
§ Hoechst AG Scientific Computing.
|| Max-Planck-Institut für Festkörperforschung.
⊗ Abstract published in *Advance ACS Abstracts,* July 15, 1997.
(1) Swarc, M.; van Beylen, M. *Ionic Polymerization and Living Polymers*; Chapman & Hall: New York, 1993.
(2) Car, R.; Parrinello, M.; *Phys. Rev. Lett.* **1985**, *55*, 2471.
(3) Dolce, T. J.; Grates, J. A. In *Encyclopedia of Polymer Science and Engineering*; Wiley: New York, 1985; Vol. 1, p 42.
(4) Penczek, S.; Kubisa, P.; Matyjaszewski, K. In *Cationic Ring Opening Polymerization, Part II: Synthetic Materials*; Advances in Polymer Science, Springer: Berlin, 1985; Vols. 68/69, 91.
(5) Penczek, S.; Kubisa, P. *Comprehensive Polymer Science*; Pergamon: Oxford, 1989; Vol. III, p 787.
(6) Kern, W.; Jaacks, V. *J. Polym. Sci.* **1960**, *48*, 399.
(7) Leese, L.; Bauber, M. W. *Polymer* **1965**, *6*, 269.

S0002-7863(97)00935-9 CCC: $14.00

and initiates polymerization (see the next section for a more detailed discussion). On the other hand, the same process can also split a longer POM chain into two fragments. A characteristic feature of TXN polymerization is that these reactions interfere with polymer growth and can have equilibrium and rate constants comparable to those of the propagation. Moreover, as is true for most polymerization procedures involving ions, these quantities depend on the nature of the solvent.[1] All these factors must be taken into account in order to control properly the kinetics and thermodynamics of the polymerization.

An intriguing process that has been the subject of many experimental studies[6−8] is the induction phase of the TXN polymerization. In this phase no visible polymer is formed, although reactions do occur. *In situ* NMR studies of $BF_3{\cdot}OEt_2$ catalyzed TXN polymerization[8] show that traces of water might play an important role as cocatalyst (generating active protons by reaction with BF_3) and that the entire process can be divided into three stages. In the first stage, called the induction phase, the concentration of free formaldehyde increases, and no net formation of polymer is observed. The second stage is characterized by the appearance of new resonances that are attributed to the formation of 1,3,5,7-tetraoxane (TEXN). Net formation of the polymer is observed only in the third stage, when the concentration of the other active species remains constant. The most important result is that polymerization starts only after a certain (temperature-independent) equilibrium concentration of formaldehyde called the ceiling concentration has been reached.[6] Although most experimental investigations so far refer to the induction phase,[6−8] its development has not yet been resolved in detail. In an attempt to gain insight into this process, we have previously carried out an *ab initio* MD simulation of the dynamics of TXN and DXL protolysis in the gas phase[9]

The present work extends the *ab initio* MD study of these and other processes to the induction period in the condensed phase. The MD system consists of a sample of TXN liquid in which an H^+ ion is introduced as a catalyst. The dynamics of progressive protolysis of TXN and the incipient re-formation of formaldehyde oligomers was examined in atomic detail. In order to characterize the thermodynamics of oligomer formation in the liquid, we have also evaluated the free-energy profile for a key reaction in the induction phase, namely the equilibrium between the cationic dimer $HO-CH_2O-CH_2^+$ and the $O{=}CH_2$ and $HO-CH_2^+$ fragments. This is the first attempt to determine with a fully nonemipirical scheme the free-energy profile for a complex process in the condensed phase.

This paper is structured as follows. In section II, after some of the basic principles of acid-catalyzed TXN chemistry as found in the literature are summarized, the MD model system is defined and justified. Section III outlines the technical aspects of the *ab initio* MD method that are relevant to our simulation, including the calculation of free energy by constrained MD. In Section IV we analyze the reaction dynamics obtained from the *ab initio* MD trajectory. In Section V we discuss the calculation of the free energy of dimerization and correlate these results with the kinetics presented in Section IV. In the appendix we report results for several ground-state properties of gas-phase monomers and oligomers, obtained both with our DFT scheme and with Hartree−Fock (HF) and post-HF methods.

(8) Collins, G. L.; Lu, N.; Yang, N.-L. In *Polymeric Materials: Science and Engineering*, Proceedings of the ACS Division of Polymeric Material, Vol. 61, ACS Fall Meeting 1989; ACS: Washington, DC, 1989; p 700

(9) Curioni, A.; Andreoni, W.; Hutter, J.; Schiffer, H.; Parrinello, M. *J. Am. Chem. Soc.* **1994**, *116*, 11251.

II. Model System

A. Reaction Steps. To define our MD system, we first briefly review the relevant reactions that take place in the cationic TXN polymerization as can be found in the literature.[3−9] We emphasize that, in spite of the coexistence of all these processes at any stage of the polymerization, three phases stand out in terms of their characteristic events.

The crucial step of the first stage of polymerization is that one TXN molecule is attacked by the cationic initiator R^+, which can be an organic or an inorganic cation[10] (in most cases the H^+ ion, originating either directly from a Brönsted acid such as $HClO_4$ or from hydrolysis by a Lewis acid catalyst such as BF_3):

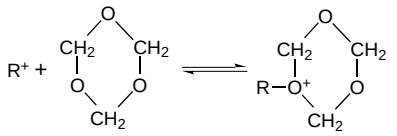

The cationic ring structure obtained in this way (eq 1) is unstable and might evolve in one of the following ways:

(i) One of the O^+-CH_2 bonds is cleaved, leading to a chain terminated by a chemically active methylene carbocation $-CH_2^+$

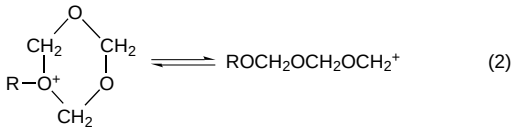

(ii) The ring opening from eq 2 is followed by a rapid decomposition into two formaldehyde molecules plus a methylenic carbocation. For a reaction in which R is an H atom, the process is

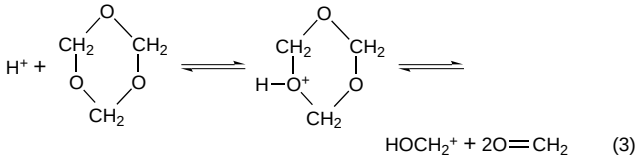

Experimental evidence[6−8] and our previous calculations of the gas phase[9] support (3) as the process dominating the induction phase. This would lead to an increase of free formaldehyde molecules.

In the second phase, the concentration of free formaldehyde becomes sufficiently high to render an alternative path possible for the evolution of protonated TXN rings (1), namely, by inserting a formaldehyde unit to form TEXN (4):

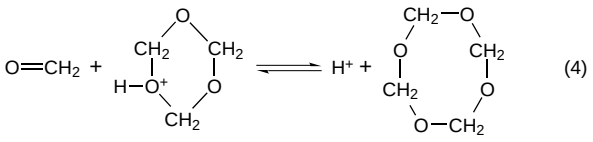

In the third phase, the concentration of free formaldehyde reaches a constant value and the growth of the polymer starts. This can proceed mainly in different elementary processes: A carbocationic terminus of a growing oligomer may attack either a free formaldehyde molecule or a TXN (TEXN) ring. In the former case, it increases its size by one unit:

(10) Collins, G. L.; Greene, R. K.; Berardinelli, F. M.; Garruto, W. V. *Polym. Sci., Polym. Lett.* **1979**, *17*, 667.

$$H(OCH_2)_nOCH_2^+ + O{=}CH_2 \rightleftharpoons H(OCH_2)_{n+1}OCH_2^+ \quad (5)$$

In the latter case, it can extend either by three or four $-CH_2-O-$ units (similar to (2)):

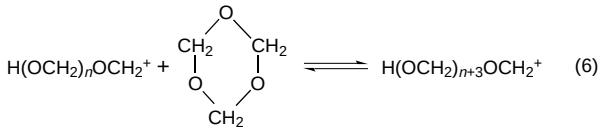

or by only one unit with the release of two or three formaldehyde molecules similar to (3). Processes 5 and 6 should predominate for the same considerations as above.

Several reactions compete with the growth of the polymer. An important degradation process is the release of formaldehyde (the reverse of (5)):

$$H(OCH_2)_nOCH_2^+ \rightleftharpoons H(OCH_2)_{n-1}OCH_2^+ + O{=}CH_2 \quad (7)$$

Another process that occurs relatively frequently during and after propagation of POMs is chain transfer (transacetalization). Chain transfer is less important in the induction phase.

B. Definition of the MD System. Reactions 1−7 summarize some of the reaction steps involved in TXN polymerization. We have taken this basic model as a guide to define the composition of our MD system in its initial state. This system consisted of a sample of TXN liquid under periodic boundary conditions and a single H^+ ion as initiator. Disregarding for the moment constraints related to system size (see below), any of the reactions 1−7 and possibly other chemical transformations could occur in the time evolution of such a system.

A component of the real system that has been left out of reactions 1−7 as well as our model, but is certainly present, is the counterion A^- of R^+. Its omission may appear to be a serious limitation of the model, considering that TXN is a poor solvent for ionic species. R^+ and A^- cannot be fully separated as in aqueous solution. This implies that the anion will remain associated in a complex $-M^+,A^-$ with the positive active end $-M^+$ of the polymer.[1]

Because A^- is the anionic residue that remains after dissociation of the initiating agent, the justification for ignoring complexation with A^- in a first approximation is closely related to the type of catalyst used. It has been proposed that in the presence of traces of water, which has a powerful effect on any stage of cationic polymerization, $BF_3{\cdot}OEt_2$ is hydrolyzed and converted into a strong protic acid:[10]

$$BF_3{\cdot}OEt_2 + H_2O \rightleftharpoons H^+BF_3OH^- + OEt_2 \quad (8)$$

When an H^+ ion is transferred from this acid to an acetal oxygen (see for example (3)), the conjugate base that remains is a large anion $BF_3{\cdot}OH^-$. Because the negative charge of such a bulky ion is distributed over a large volume, the ion is only loosely bound to the organic cation, possibly separated from it by a layer of solvent. This is one of the reasons why for cationic polymerization, initiators that produce large anions are preferable because then the effect of the counterion on the propagation can be assumed to be minimal.[1] Relying on this argument, we have simply eliminated the counterion for our simulation.

Not only the composition, but also the size, of the MD system can impose limitations on the range of phenomena the model can describe. The initial state of the MD system is set up with seven TXN molecules in a cubic periodic box with a length of $L = 9.865$ Å, corresponding to a density of 1.09 g-cm^{-3}. With a total of only 21 formaldehyde monomers, the effects of the boundary on the basic chemical reactions summarized in the previous section cannot be neglected but are not expected to be so serious that they would completely inhibit these processes.

There is one important aspect of the physical chemistry of TXN polymerization that the *ab initio* MD system will fail to reproduce. The polymer is not soluble in the mixture of trioxane and formaldehyde and crystallizes as soon as it is formed. Hence, the polymerization reaction proceeds at a solid−liquid interface and is essentially heterogeneous (see, e.g., ref 4). The free energy of solidification adds to the thermodynamic driving force of polymerization, without which the synthesis of POMs of high molecular weight might not even be feasible.[4] Clearly, the study of this phenomenon requires very large systems and is beyond the scope of our *ab initio* MD simulation.

III. *Ab Initio* MD Method

A. Approach to the Electronic Structure. In the *ab initio* MD method, the electronic structure is determined by a DFT-based computational approach. For a review of the *ab initio* MD methodology the reader is referred to ref 11; for reviews of DFT see e.g., refs 12 and 13. The energy functional used here is of a gradient-corrected (semi)local form. It consists of a leading term in the local density approximation (LDA) and the gradient correction (GC) for exchange developed by Becke.[14] With this relatively simple extension, DFT predictions for formation (dissociation) energies are improved substantially.[15,16] The Becke GC for exchange was also shown to be crucial for a realistic description of hydrogen bonding in condensed systems (for liquid water, see refs 17 and 18. In the present application to chemistry of liquid TXN, we have used this functional without a further GC for correlation. This density functional is usually referred to as B.

Only valence electrons are considered explicitly, and angular momentum-dependent, norm-conserving pseudopotentials are employed to account for interactions between the valence electrons and the atomic cores.[11] The potentials for carbon and oxygen were generated using the Troullier−Martins procedure.[19] The l components of the pseudopotentials are also defined by an effective core radius, which determines the degree of softness of the potential, 1.23 au for C and 1.1 au for O. The hydrogen ion is represented by a simple analytic pseudopotential which is essentially a softened Coulomb potential with a core radius of 0.25 au. An important technical feature of the Car−Parrinello method is the plane−wave basis set used to expand the electronic wave functions. In the present calculation, we have adopted an energy cutoff at $E_c = 70$ Ry for this expansion. Results for structural and energetic properties of formaldehyde and some of the relevant acetals with the present scheme are reported and discussed in the appendix.

B. Boundary Conditions. The constant volume MD simulation of the TXN liquid is performed in a periodically replicated simple cubic cell. A net total charge of the MD cell,

(11) Galli, G.; Parrinello, M. In *Computer Simulation in Materials Science: Interatomic Potentials, Simulation Techniques and Applications*, Meyer, M., Pontikis, V., Eds.; NATO ASI Series E, Vol. 205; Kluwer: Dordrecht, 1991; p 283.
(12) Parr, R. G.; Yang, W. *Density-Functional Theory of Atoms and Molecules*; Oxford University Press: Oxford, 1989.
(13) Gunnarson, O.; Jones, R. D. *Rev. Mod. Phys.* **1991**, *61*, 689.
(14) Becke, A. D. *Phys. Rev. A* **1988**, *38*, 3098.
(15) Becke, A. D. *J. Chem. Phys.* **1992**, *96*, 2155.
(16) Johnson, B.; Gill, P. M. W.; Pople, J. A. *J. Chem. Phys.* **1993**, *98*, 5612.
(17) Laasonen, K.; Sprik, M.; Parrinello, M.; Car, R. *J. Chem. Phys.* **1993**, *99*, 9081.
(18) Sprik, M.; Hutter, J.; Parrinello, M. *J. Chem. Phys.* **1996**, *105*, 1142.
(19) Troullier, N.; Martins, J. *Phys. Rev. B* **1991**, *43*, 1993.

as in our acid model system (see section II.B), is in principle incompatible with periodic boundary conditions because of the divergence of the electrostatic interaction energy. In condensed-phase simulations this complication is usually circumvented by compensating the physical excess charge with a homogeneous background distribution. This is also our strategy for the study of the reactive liquid.

To determine equilibrium structures and energies of ionic clusters in vacuum, this charge compensation method is not a satisfactory solution. Moreover, in a lattice of neutral polar molecules the long-range interactions can also be a serious perturbation if this system is meant as an approximation to the isolated molecule. These cases call for a rigorous approach to eliminate the interaction between periodic images generated by expansion in Fourier components. In our study of protonated gas-phase molecules, appendix A, we have applied a numerical screening technique similar to the method proposed in ref 20.[20] For a calculation supporting the claim that the asymptotic electrostatic dipole−dipole interaction for a pair of polar molecules is indeed recovered with this method, we refer to the section on the water dimer in ref 18.

C. Molecular Dynamics. The instantaneous electronic ground state as it evolves during the MD simulation is obtained in the *ab initio* MD approach by treating the Fourier coefficients of the electronic wave functions as an additional set of classical dynamic variables that interact with the ionic coordinates.[2,11] Provided the response of these electronic degrees of freedom to changes in the positions of the ions is sufficiently fast, the system remains close to the Born−Oppenheimer surface, and the motion of ions reproduces the adiabatic dynamics at finite ionic temperature (for a discussion of this important point see refs 21 and 22). The freedom in specifying the fictitious mass parameter μ of the classical degrees of freedom representing the electronic states gives limited control over the value of the time step Δt used in the MD iteration. Another numerical coefficient that directly affects the value of Δt is the plane wave cutoff E_c. The reason is that the high-frequency end of the spectrum of the (classical) motion of the electronic degrees of freedom is dominated by harmonic restoring forces derived from the (quantum) electronic kinetic energy.

For an E_c of 70 Ry and a μ between 500 and 1000 au, time steps for a stable dynamics vary from 0.1−0.15 fs. These values of Δt, which are rather short on the time scale of the molecular motion, can be increased at the cost of affordable additional CPU time by scaling the effective mass for a $\boldsymbol{G}$ component by a G -dependent factor that increases inertia at high G.[22] Further gains in computational efficiency can be achieved by treating the approximately harmonic motion of these expansion coefficients as the fast subsystem in a reversible multiple time-step propagator.[22] We have employed both of these methods for an electronic system with $\mu = 1100$ au. In addition, the mass of the H atoms was set to the value for the deuterium isotope to improve the adiabatic separation of the motion from the electronic and ionic degrees of freedom. In this way, the time step for the MD integration was increased to 0.34 fs.

D. Free-Energy Calculation. A crucial argument in the analysis of our simulation results is the calculation of the free-energy changes for an elementary step in the reaction, namely, the formation of an acetal CO bond of the dimer in the liquid. The computational approach we have applied is adapted from a method developed for classical MD studies of the dissociation of ion pairs in polar solvents.[23] The scheme in ref 23 uses the method of constraints to determine the solvent-averaged force $f^{(S)}(r)$ between two solvated ions A and B for a series of increasing distances $r = r_{AB}$ starting from the separation r_0 of the bound ion pair. The relative free energies $\Delta F(r)$ of these states are then obtained by integrating the solvent-averaged force (also called the mean force)

$$\Delta F(r) = F(r) - F(r_0) = -\int_{r_0}^{r} \mathrm{d}r'\, f^{(S)}(r') \qquad (9)$$

The MD implementation is based on the relation between the mean force and the force of constraint required to keep the ion pair at a fixed separation $r_{AB} = r$ during the MD simulation. For the simple case of a distance constraint $\sigma(r_{AB}) = r_{AB} - r = 0$, the force of constraint is equal to the corresponding Lagrange multiplier $\lambda(r)$,[24] and we have

$$\langle \lambda(r) \rangle = f^{(S)}(r) = -\left\langle \frac{\partial V}{\partial r_{AB}} - \frac{2k_B T}{r_{AB}} \right\rangle_{r_{AB}=r} \qquad (10)$$

The brackets denote an ensemble average over all configurations of solvent atoms and ions A and B with the condition that the ions be at a specified distance r_{AB}. V is the potential energy function for the complete system. The second identity in eq 10 states that the mean force can be resolved into an average radial force derived from the model for the particle interactions and a temperature-dependent correction term. We have added the second relation in eq 10 mainly to emphasize that this correction term, which has caused some confusion in the literature, is accounted for by the force of constraint. In fact, this term can be identified as the average of an inertial radial force (the centrifugal force) which, superimposed on the potential radial force, is automatically compensated by the method of constraints[24]

Calculation of the free energy consists of determining the average Lagrange multiplier $\lambda(r)$ for a discrete set of interionic distances $r_{AB} = r$ by performing a constrained MD run for each of these states. In practice, the value of r is increased in small increments using the final state of the previous simulation as the initial configuration for the next. The relative free energies for the set of r values are obtained as a discrete approximation to the integral

$$\Delta F(r) = -\int_{r_0}^{r} \mathrm{d}r' \langle \lambda(r') \rangle \qquad (11)$$

The validity of eq 11 is not dependent on the interatomic forces being derived from a parametrized model. Hence, the method of constraints can be generalized without modification to an *ab initio* MD simulation of chemical reactions. We simply substitute for the ions A and B the reactive atoms between which a chemical bond is formed. The role of the solvent is played by all other atoms in the system including those that may already be bonded to A and B. Similar to the classical application, fluctuations of these "solvent" degrees of freedom modulate the direct force responsible for the bonding between A and B and should, therefore, be appropriately sampled. Hence, the minimum duration required for a constrained MD run depends on the time scales of the motion in the system. We will return to this issue in our discussion of the results for the TXN system.

IV. Dynamics of the Reactive Liquid

A. Time Evolution of Composition. The initial state of the model MD system specified in section II.B was prepared in

(20) Barnett, R. N.; Landman, U. *Phys. Rev. B* **1993**, *48*, 2081.
(21) Pastore, G.; Smargiassi, E.; Buda, F. *Phys. Rev. A* **1991**, *44*, 6334.
(22) Tuckerman, M. E.; Parrinello, M. *J. Chem. Phys.* **1994** *101*, 1302; 1316.
(23) Ciccotti, G.; Ferrario, M.; Hynes, J. T.; Kapral, R. *Chem. Phys.* **1989**, *129*, 241.
(24) Carter, E. A.; Ciccotti, G.; Hynes, J. T.; Kapral, R. *Chem. Phys. Lett.* **1989**, *156*, 472.

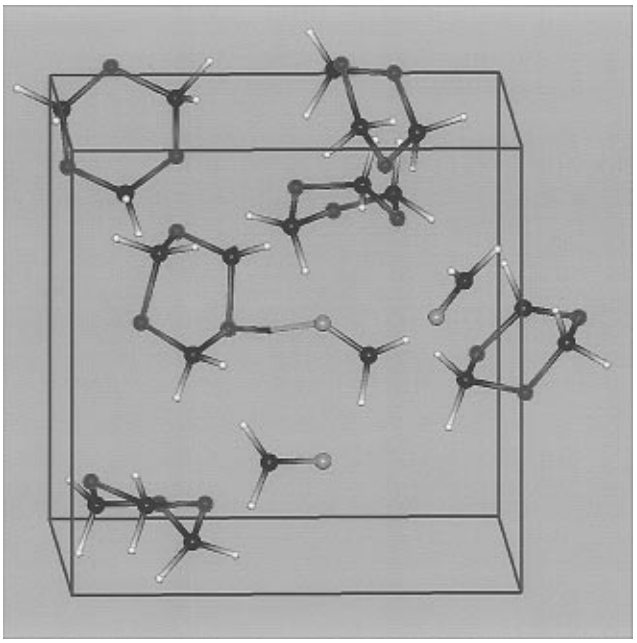

Figure 1. Snapshot of the MD sample of trioxane liquid after the first TXN protolysis. Carbon atoms are gray; alkyl hydrogen atoms, white; acetal oxygen atoms, red; carbonyl oxygen atoms, yellow. Pictured is a state just after the transfer of the excess proton (blue) from a formaldehyde oxygen, to which it is still linked by a hydrogen bond (green), to an acetal oxygen of a trioxane molecule. This molecule will be fragmented during the next period of 1 ps. The red lines outline the periodic cubic MD cell.

two stages. First, a classical pair-potential MD run was used to generate a liquid sample of seven TXN molecules at a high temperature (∼500 K) in a slightly compressed simple cubic periodic cell of length $L = 9.436$ Å. The *ab initio* MD was switched on, and the microcanonical system of pure TXN liquid was equilibrated for a period of ∼1.0 ps. The next step was to insert the excess proton. The H^+ ion was placed next to an acetal oxygen of a TXN molecule in a configuration corresponding to protonated TXN (see appendix A.1). After the simulation was restarted, the protonated TXN was fragmented almost instantly, i.e., within ∼0.5 ps. This agrees well with our results for the gas phase.[9] The equilibration of the liquid + proton was continued for a duration of 4 ps. No further decomposition of TXN was observed. The pressure in the fixed-volume MD cell can be expected to increase with progressive TXN decomposition because three OCH_2 monomers released by the TXN occupy a larger effective volume than in their former state when they were bound in a cyclic trimer. To compensate for this increase in pressure we have empirically increased the sample volume to a value larger than the volume of a sample with experimental density of liquid trioxane by 15%. This corresponds to a cell length L of 9.865 Å. Figure 1 shows a configuration of the system, prior to further reactive events, consisting of six TXN, two OCH_2, and one $HOCH_2^+$ molecule. During the subsequent microcanonical run of 12 ps, the temperature fluctuated between $T = 400$ and 600 K.

The evolution of the MD system can be partitioned into two intervals. In the first 5 ps, three of the six TXN were dissociated in OCH_2 by a rapid succession of proton transfers and cleaving of CO bonds, according to (3) in section II.A. The three surviving TXN molecules remained stable until the end of the run. A plot of the population N of chemically different O atoms as a function of time (Figure 2) clearly distinguishes between the two phases in the reactive dynamics. The two types of oxygen (O_{ac} and O_{cy}) were assigned by geometric and topological criteria. An O atom is identified as an acetal oxygen if there

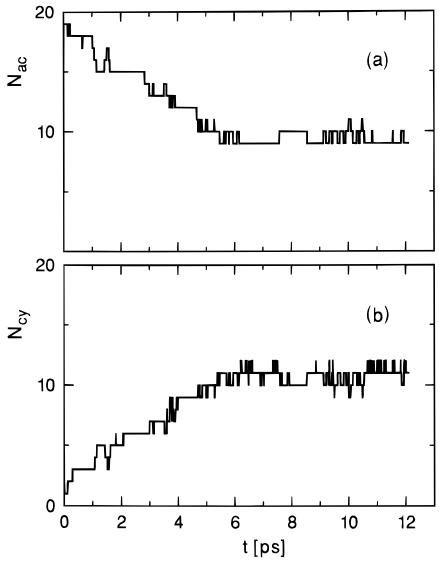

Figure 2. Time evolution of chemical composition of the reactive TXN−formaldehyde mixture with an H^+ ion added: (a) Number of acetal oxygen atoms in the sample at time t and (b) the same as in part a for the number of carbonyl oxygen atoms.

are two carbon atoms within a radius of 1.95 Å. An O atom counts as a carbonyl oxygen if it is part of a molecule consisting of exactly four atoms. After a steep decrease of $N_{O_{ac}}$ and the complementary increase of $N_{O_{cy}}$, both populations reach a plateau value of about 10 at 5 ps.

Another property that can be used to quantify the difference in the nature of the chemical reactions in the two phases is the weight of the molecule with the hydroxyl end. This molecule, because of the acidity of the OH group, is a center of chemical activity in our system (see section II.A). The histogram of the number of atoms n_+ in the cationic molecule obtained from the fluctuations of this quantity over the first 5 ps and the distribution of the remainder of the trajectory are shown in Figure 3a,b, respectively. The $n_+ = 5$ and $n_+ = 9$ columns correspond to the protonated monomer $HOCH_2^+$ and dimer $HOCH_2OCH_2^+$, respectively. For protonated TXN and the linear trimer that is formed by ring opening, we have $n_+ = 13$. For some configurations we find a H^+ ion that is not bonded to an oxygen, yielding $n_+ = 1$. This unbound proton is not really "free" but is in the process of being transferred from one O to another (for further discussion of this issue see section IV.B).[1] The actual number of these protons in transition is, of course, rather sensitive to the OH bond criterion used (1.2 Å).] The change in distribution of n_+ before and after 5 ps is significant. During the initial phase of the run (Figure 3a), the probability of finding a monomer or dimer is lower than that of finding a TXN or a trimer. In Figure 3b, on the other hand, the monomer and dimer species clearly dominate. In the following two sections we will analyze the atomic motion in detail in order to understand the chemistry underlying Figures 2 and 3.

B. Proton Transfer and Protolysis. As is clear from the brief outline of acid-catalyzed TXN chemistry in section II.A, the two key species driving the chemical reaction are the H^+ ion inserted at the start of the MD run and the carbocation partially localized on a CH_2^+ group. Even if no longer ionic, the original proton can be tracked on its way through the liquid. This is particularly straightforward in our system with its simplified composition because the (former) H^+ will be the only H atom that is not bonded to a carbon. Hence, without any risk of ambiguities, we can generalize the terminology of an excess H to denote the hydrogen not bonded to a carbon. This excess H atom is bound most of the time in the hydroxyl group

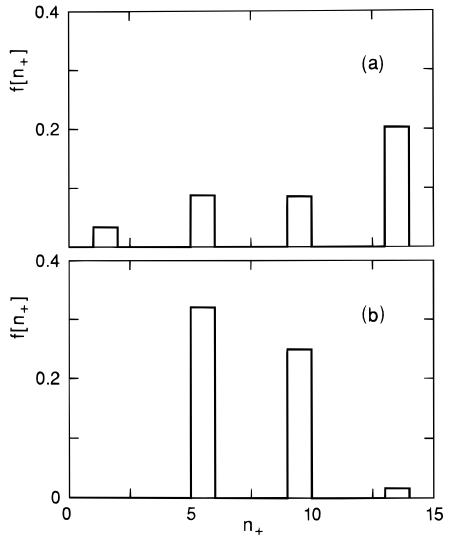

Figure 3. Distribution of the number of atoms in the cationic molecule containing the acid OH group: (a) histogram evaluated over the first 5 ps of the trajectecory; (b) histogram for the trajectory after 5 ps (see Figure 2). The left-most column in part a corresponds to an unbound H^+ atom. Normalization is calculated from the full 12 ps run.

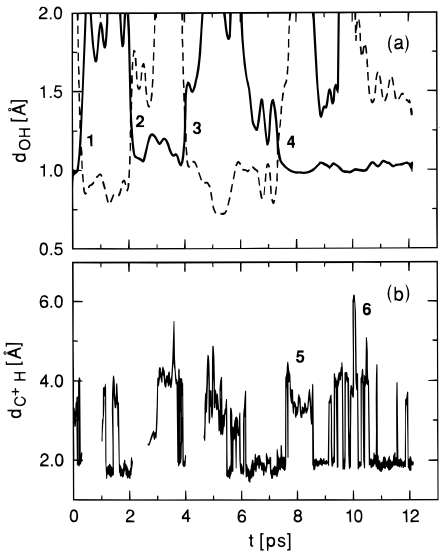

Figure 4. Distances between reactive atoms as a function of run time *t*. Part a displays the distance of the excess proton and nearby O atoms. The trajectories are represented by lines alternating between solid and dashed in the sequence in which the O atoms are approaching and receding. Numbers label proton transfer events. Part b displays the distance between the carbocation and the H atom of the acid hydroxyl group (excess proton). In the intervals without a curve, the carbocation is absent. Numbers label events referred to in the text. The high-frequency oscillations in part a have been removed by smoothing.

of the $HOCH_2^+$ monomer or in the tail of a linear acetal chain. A third type of H bonding site is the oxonium (O^+) atom in a closed protonated TXN ring (see, e.g., (3)). The H atom of such an OH or O^+H group is hydrogen bonded most of the time to either a carbonyl or acetal O. Occasionally, the proton is transferred, which switches the chemical and physical hydrogen bond from one oxygen to the other. This is illustrated in Figure 4a where we have plotted the variation in time of the distances of O atoms in the vicinity to the excess H with respect to this atom. Stationary OH distances are distributed around the value of $d_{OH} \approx 1$ Å, the chemical OH bond, and $d_{OH} \approx 1.7$ Å, which is the OH separation typical for a hydrogen bond. Where trajectories coming from these two regions intersect, a proton transfer occurs. Four of these events can be seen in Figure 4a, labeled according to their sequence in time. The exchange is almost instantaneous. Only during event 4 is there a brief delay of about 0.5 ps (see below).

If such a transfer of the H^+ ion takes place from a protonated formaldehyde $HOCH_2^+$ to an acetal O of TXN it can induce breaking of a CO bond and initiate decomposition of the TXN molecule (reaction 3). In order to reveal a correlation between the attachment of a proton and a ring opening we have compared the location of the carbocation C^+, i.e., the C atom in the terminal methylene group of a linear molecule carrying positive charge, to the position of the excess H. Similar to the procedure for finding the acetal and carbonyl O discussed in section IV.A, we applied a topology rule to identify the particular carbon atom that assumes the function of the C^+ in a given configuration. If a C atom is bonded to only one O atom and is part of a molecule containing an OH group, it is the carbocation C^+. Figure 4b gives the history of the distance d_{C^+H} of C^+ with respect to the excess H. The "baseline" of $d_{C^+H} \approx 19$ Å in the time fluctuations corresponds to a C^+H pair bound in $HOCH_2^+$. The geometry of the monomer is a fairly rigid one, constraining the C^+H separation to a well-defined range of values. If, on the other hand, the carbocation forms the end of a linear acetal dimer or trimer, the C^+ has the freedom to move farther away from the excess H. This is the explanation of the intervals with larger C^+H distances in Figure 4b. The frequent discontinuities of ~2 Å cannot be interpreted as anomalously fast physical transport over this distance but correspond to the breaking of a CO bond, which forces one C atom to take over the role of carbocation from another C atom.

The interruptions, in which no carbocation could be detected, are a further important characteristic of the trajectory and are clearly indicative of the chemistry going on in our system. During these time intervals, the H^+ is bonded to a closed TXN ring. The start of C^+ eclipses corresponds to events 1−3 when an acetal O in a TXN ring is attacked by the hydroxyl end of $HOCH_2^+$ followed by a transfer of the H^+ ion. Reappearance of the C^+ occurs after ~0.7 ps, accompanied by the simultaneous sudden increase of d_{C^+H}. This marks the moment at which an adjacent CO bond has been cleaved, and the TXN ring is in the process of opening. In all three cases the reaction continued with the successive breaking of further acetal bonds, ending with dissociation of the TXN molecule into three monomers. The kinetics of this spontaneous reaction is virtually identical to the vacuum decomposition process described in our previous study (for details see ref 9). The time scale in the liquid can be estimated from the relaxation of d_{C^+H} in Figure 4b to the 1.9 Å $HOCH_2^+$ value. All three TXN molecules have been broken up within 1 ps after ring opening. In Table 1 we have summarized some of these time constants. Whereas events 1−3 in Figure 4a are proton transfers to an acetal O in a TXN molecule, event 4 is a proton exchange across the hydrogen bond between $HOCH_2^+$ and a OCH_2 monomer. The oscillations in d_{OH} preceding the final transfer are the signature of the formation of an evanescent proton-bonded formaldehyde dimer. In the gas phase this dimer is stable. Its structure is shown in Figure 5a. The dimer observed in the simulation of the solution existed only for a fraction of a picosecond.

C. Re-formation of Oligomers. At first glance the saturation of composition in Figure 2 is what one would expect for a chemical reaction in a closed system, namely a relaxation to chemical equilibrium between components. The opposite response of the $N_{O_{ac}}$ and $N_{O_{cy}}$ dynamics during the first 5 ps suggests that it takes only this long for the protolysis to convert the excess TXN into formaldehyde and, hence, from that moment on, that populations are stationary. However, analysis

Table 1. Characteristic Times and Diffusion[a]

	react.	form.	TXN
τ_{ro}, ps	1		
τ_{dc}, ps	2		
τ_{CO}, ps		0.4	3
τ_{HH}, ps		0.3	
D_O, Å^2 ps^{-1}		0.4	0.4
D_{H^+}, Å^2 ps^{-1}	0.7		

[a] Time (τ) and diffusion constants (D) determined from the 12-ps trajectory of free dynamics. Properties characterizing the reaction dynamics (react.) are compared to the time scale of the motion of formaldehyde (form.) and trioxane (TXN) molecules in the solution. The parameters τ_{ro} and τ_{dc} are the times from protonation of a TXN molecule to the ring opening and full decomposition into monomers, respectively. The parameters τ_{CO} and τ_{HH} are orientational relaxation times of the CO bond and the vector connecting two H atoms, respectively. Statistical errors are of the order of 30%.

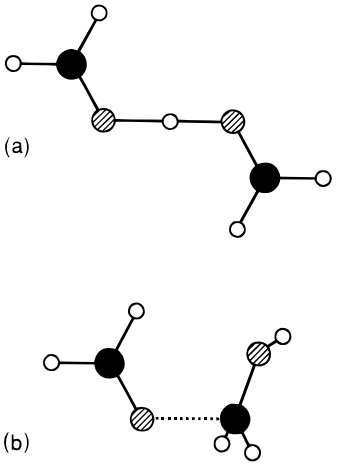

Figure 5. Dimers of formaldehyde, OCH_2, and its protonated derivative, $HOCH_2^+$. Shown are the stable gas-phase structures of two configurations observed during the *ab initio* MD simulation of the liquid mixture. Carbon atoms are black; oxygen atoms, gray; and hydrogen atoms white. Part a shows hydrogen-bridged dimer with symmetric hydrogen bond. The ~1.5 ps periods of rapid OH distance fluctuations preceding event 4 in Figure 4a are attempts to form this dimer, which turns out to be unstable in the solution. Part b shows dimer bonded by a carbon oxygen bond (dashed line). The formation of this dimer is responsible for the increased C^+-H distances during events 5 and 6 in Figure 4b. The length of this CO bond is the distance that is constrained in the calculation of the free energy of dimer formation discussed in Section V.A.

of the spatial distribution of the species in the system revealed that the TXN formaldehyde mixture that is produced is inhomogeneous. All formaldehyde is concentrated in the same limited region of the MD cell and is, moreover, clustered around the $HOCH_2^+$. A simple way of probing this spatial variation in composition is to count the number of acetal and carbonyl O atoms present at a given moment in a spherical volume with radius r_c with the carbocation C^+ as center. We will denote these coordination numbers by $n_{O_{ac}}$ and $n_{O_{cy}}$, respectively. Figure 6 shows the change in coordination for a value of r_c = 4 Å as the reaction proceeds. The values of $n_{O_{ac}}$ and $n_{O_{cy}}$ have been set to zero when the carbocation is absent (see Figure 4 and the discussion in section IV.B). During the three protolysis events in the first 5 ps, $n_{O_{ac}}$ and $n_{O_{cy}}$ are essentially equal. After TXN decomposition has come to an end, carbonyl O begins to accumulate around the carbocation.

There are two well-defined intervals later in the run, where for a short moment the values of $n_{O_{ac}}$ and $n_{O_{cy}}$ approach each other again (Figure 6). These fluctuations closely match in time the last two series of peaks in Figure 4b, which we have indicated by the labels 5 and 6. As discussed in the previous

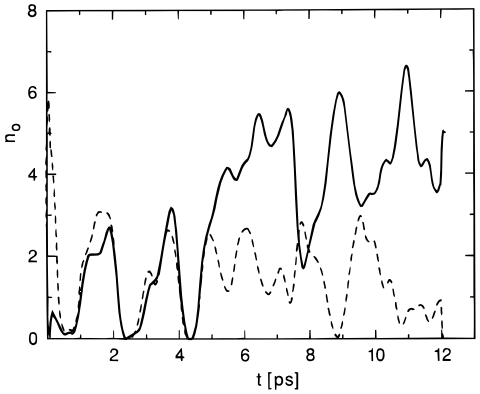

Figure 6. Number of carbonyl O atoms (solid) and acetal O atoms (dashed) within a radius of 4 Å from the carbocation as a funtion of time. High-frequency fluctuations have been removed by smoothing.

section, the discontinuities in the C^+H separation signal chemical activity. From the animation of events 5 and 6 one can see that what occurs are attempts at re-formation of a $HOCH_2$-OCH^+_2 dimer. This reaction, depicted in Figure 5b, is accompanied by an abrupt displacement of the C^+ over the length of a formaldehyde monomer, which is reflected in a 2 Å increase in d_{C^+H}. The dimers formed are not stable and break up again after 1 or 2 ps. The d_{C^+H} = 6 Å spike standing out at t = 10 ps in Figure 4b is the signature of a very short-lived trimer. The nature of the CO bond in the protonated dimer and trimer will be discussed in appendix A.1.

D. Evaluation of Dynamics Results. Considering the ease with which TXN molecules are protolyzed in the first phase of the simulation, the instability of the oligomers formed in the second phase would be no real surprise if the thermodynamic state was constant. In that case, the two processes are essentially the same chemical reaction in opposite directions under similar thermodynamic conditions. However, temperature and pressure are not controlled in the simulation. In particular the pressure in the fixed-volume MD cell increases with progressive TXN decomposition, as mentioned in section IV.A. A further complication for a direct comparison of beginning and end of the trajectory is the growing inhomogeneity in the spatial distribution of formaldehyde discussed in section IV.C. However, the effect of the modified thermodynamic state is apparently insufficient to reverse the reaction in the "bubble" of accumulating formaldehyde.

Ignoring then the uncertainties involved in specifying the thermodynamic state of the system, the primary issue concerns the apparently modest value of the thermodynamic driving force of the reactions. The fact that we observe any spontaneous chemical process at all on a picosecond time scale implies that these reactions cannot be endothermic with reaction energies in excess of a few k_BT. The same upper limit holds for the estimate of the free-energy barriers that separate reactant and product states. Nor can the reaction be strongly exothermic because a substantial release of reaction heat would have been detected by a clear increase of temperature over the 12 ps constant energy run.

V. Thermochemistry of Acetal Bond Formation

A. Free Energy of Dimerization. A fundamental step toward understanding the thermochemistry and kinetics of a reaction is to examine the relative free energies of states along the reaction path from reactant to the product via possible transition states. In a series of independent calculations we have determined the free-energy profile for breaking of the CO bond of the dimer using the method of constraints outlined in section

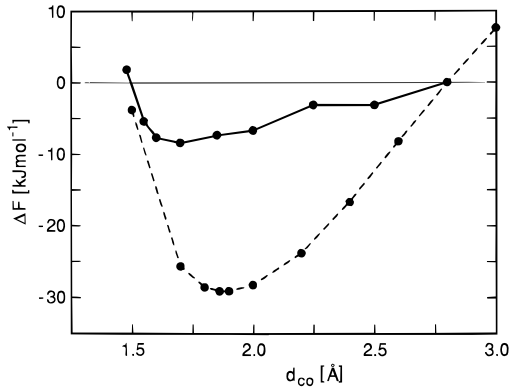

Figure 7. Free energy for dissociation of a $HOCH_2OCH_2^+$ dimer into OCH_2 and $HOCH_2^+$ monomers as a function of the acetal CO bond length as determined by constrained *ab initio* MD simulation. The solid curve gives the result for a dimer in a TXN−formaldehyde mixture at 300 K (for details see text). The dashed curve is the result for a dimer in vacuum at low temperature. The free energies are measured relative to the value at $d_{CO} = 2.8$ Å.

III.D. The length of the bond between the acetal C and O, d_{CO} in Figure 5b, was constrained and the average Lagrange multiplier λ was evaluated for a series of values of the CO distance varying from $d_{CO} = 1.5$ to 2.8 Å. Starting with the smallest value, the calculations were performed in sequence incrementing d_{CO} in steps by stretching it by a small amount in the final configuration of the preceding constrained run. The temperature was controlled by a Nosé thermostat acting on the ionic degrees of freedom.[21,22] The variation of free energy with d_{CO} was obtained from the set of average λ values by means of numerical integration (see eq (11) and comments in section III.D).

For later comparison with the liquid-phase results we first computed the free energy of the dimer in vacuum at a temperature of 50 K. Low-temperature vacuum calculations can also serve as a way of testing the accuracy and validity of free energies obtained from constrained *ab initio* MD runs. For comparison with static calculations of the binding energy, the reader is referred Appendices A.1 and A.2. The resulting free energies are plotted in Figure 7 as differences ΔF with respect to the $d_{CO} = 2.8$ Å point. At these low temperatures, entropy effects are minor. Hence $\Delta F \approx \Delta E_0$, where E_0 is the adiabatic ground-state energy obtained from the DFT calculation. We verified that this relation was satisfied with deviations of less than 2 kJ mol^{-1}.

In the liquid, the initial configuration was created by bringing together the $HOCH_2^+$ and a nearby OCH_2 in the final configuration of the trajectory of free dynamics and fixing the distance between the C of the protonated formaldehyde and the carbonyl O of the formaldehyde at a value of $d_{CO} = 1.55$ Å (Figure 5b). The average temperature and density of the constrained runs were slightly different than the values specified in Section IV.A. The temperature was kept at 300 K, and the edge of the periodic simple cubic cell was adjusted to $L = 10.1$ Å, which is more suited for our final sample containing 12 formaldehyde molecules (see discussion in section IV.A).

The critical parameter for the accuracy of free energies determined by the method of constraints is the length $\Delta\tau$ of a run at a given value of the constrained reaction coordinate (see discussion in section III.D). The simulation of the $d_{CO} = 1.55$ Å system, the first in the series, was continued for $\Delta\tau = 4.5$ ps. The duration of this period turned out to be more than sufficient to estimate equilibration times as well as the $\Delta\tau$ required for convergence of the average of the Lagrange parameter. In fact, after only 2 ps of accumulation, the estimated λ was close to the average over the full 4.5 ps. Subsequent trajectories had shorter lengths varying between $\Delta\tau = 1.5$ and 2.5 ps for a total of 21 ps. Further support of the claim that time scales of this order are adequate for the determination of free energies in our system is provided by the relaxation times for the formaldehyde dynamics in Table 1, which are in the vicinity of 0.5 ps. The results obtained for ΔF in the liquid are given by the second set of data in Figure 7.

B. Correlation with Structure and Dynamics. The free-energy profiles in Figure 7 exhibit several interesting features that can explain most of the questions raised in the discussion in section IV.D. In both the liquid- and the gas-phase environment the CO bond breaks without encountering an activation barrier. However, the most striking result is perhaps the large difference in free energy of the liquid compared to that of the gas phase. Another significant observation is that the intermolecular interaction between the dissociation products is long-ranged. The energy of 37 kJ mol^{-1} that needs to be provided to separate the OCH_2 and $HOCH_2^+$ fragments in the gas phase over a distance of $d_{CO} = 3.00$ Å is less than half of the total binding energy (see Table 5 of appendix A.2). The curve in Figure 7 suggests that the asymptotic value is approached at considerably higher values of d_{CO}.

The absence of a barrier is related to the heterolytic character of the reaction. When the bonding between C and O is lost, both electrons of the pair that made up the anomalous "acetal" σ bond (see appendix A.1) stay with the OCH_2 fragment, thus restoring a carbonyl group. This is accompanied by the localization of the positive charge on the other fragment. As with the dissociation of a polar dimer into ion pairs, the ionization of the less electrophilic partner is a uniform process without the intervention of level crossings that create energy barriers. The slowly decaying tail found by the vacuum calculation also fits into this picture. The positive charge of $HOCH_2^+$ is localized mainly on the methylene group. The resulting charge−charge-induced dipole interaction is long-ranged and decreases only gradually when the fragments recede to larger distances.

In the liquid, the situation is more complex. The nature of the bonding in the protonated dimer is similar to that in the isolated one, although a greater participation of the configuration **1** (reaction 12 of appendix A.1) can be inferred from the shorter CO distance at the free-energy minimum (Figure 7). The partial delocalization of the positive charge in the dimer compared to its strong localization after dissociation also helps explain the interaction with the rest of the system and its effect. The carbonyl O that is eventually released has to compete with O atoms of other formaldehyde molecules. In Figure 6 we have seen already that the number of OCH_2 molecules in the local environment in which the dimerization takes place is appreciable. More detailed information about C^+O correlations is given in Figure 8, which shows the radial distribution $g_{C^+O_{Cy}}(r)$ of the carbonyl O with respect to the C^+ atom. The relevant structure has its maximum at 3 Å, which is well beyond the range of chemical bonding. This peak is missing in the generic CO radial distribution $g_{CO}(r)$ (also displayed), confirming that the charge-induced polarization builds up a coordination shell of formaldehyde molecules around the carbocation, pointing with the O end of the carbonyl bond toward the C^+. This shell extends to $r \approx 4$ Å and contains about four O atoms.

In conclusion, the reduction of the free energy of formation in the liquid can be attributed to two factors: (1) the more efficient solvation effect for the protonated formaldehyde product compared to that of the dimeric carbocation, owing to the different degree of positive charge localization and (2) the

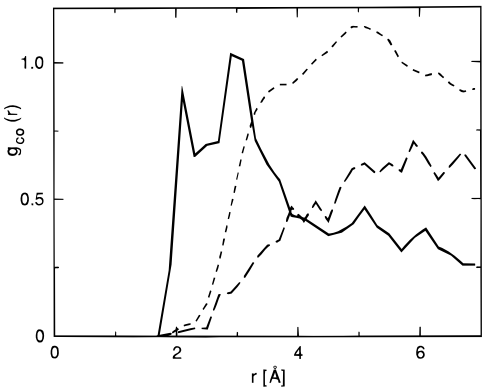

Figure 8. Bonding-selective carbon−oxygen radial distribution functions in the reactive TXN−formaldehyde mixture. The solid and dashed curves refer to the carbocation−carbonyl oxygen and carbocation−acetal oxygen distributions, respectively. The dotted curve is the generic carbon−oxygen radial distribution. The function g_{C^+} and the other radial distributions are averages over the full 12 ps free-dynamics trajectory. The abrupt cutoff below 2 Å in $g_{C^+O_{Cy}}(r)$ is a consequence of our geometric definition of a carbonyl O and cation C (see section IV.A).

screening of the effective attraction of the two fragments owing to the presence of strongly polarizable formaldehyde molecules surrounding the C^+ center.

Entropy effects, which are more difficult to assess, can also play a role. The resulting free energy gained by dimerization in the liquid (Figure 7) is of the order of 10 kJ mol^{-1}, which is only a fraction of the binding energy of 102 kJ mol^{-1} in the gas phase (see appendix A.2). This low value is four times higher than that of k_BT at 300 K and can be easily supplied by thermal fluctuations. Moreover, the reaction is activationless. Hence, the condensed-phase thermodynamics we find from the constrained MD runs is consistent with the kinetics of the free-dynamics run in which we see the dimerization reaction occurring in both directions on a picosecond time scale.

In our analysis of the interaction of the carbocation and carbonyl oxygen, the bond topology selective radial distributions proved to be a convenient probe of chemical activity. We also used this method to explore possible other reactions in which the carbocation is engaged or attempting to engage. Candidates in the MD system are the reactions of (1)−(3) described in section II.A, with *R* being the protonated formaldehyde. The third function shown in Figure 8 represents the radial distribution $g_{C^+O_{ac}}(r)$ of the acetal oxygens with respect to C^+. This distribution is a record of intermolecular correlations only, i.e., the acetal O atoms, which are part of the molecule containing the C^+, are excluded. Comparing $g_{C^+O_{ac}}(r)$ to $g_{C^+O_{cy}}(r)$ we see that the acetal O atoms are much farther removed from the C^+, and we can rule out any reactive encounter between the C^+ and acetal O atoms during simulation. The reason for this can be low reactivity, which is further reduced as a result of screening by the carbonyl O atoms which have a high affinity for the carbocation. Another reaction that occurs during the induction phase under experimental conditions is the OCH_2 insertion into TXN producing TEXN (reaction 4 in section II.A). This process could not be observed during the MD simulation, which is most likely too short for such a complex event to occur spontaneously.

VI. Summary and Discussion

The results of the *ab initio* MD study, which are relevant for understanding of the chemistry of acid-catalyzed polymerization in the induction phase, can be summarized as follows. Protolysis of TXN in a liquid mixture with a low concentration of formaldehyde monomers proceeds on a picosecond time scale. It is initiated by the transfer of a H^+ ion from a protonated formaldehyde to an acetal O atom of TXN, which leads to ring opening and subsequent complete decomposition within 2 ps. This event is repeated again within a few picoseconds by the transfer of the H^+ ion of the protonated monomer fragment to another TXN nearby, until a pocket of OCH_2 is formed enveloping the $HOCH_2^+$. From this moment on, which in the MD sample occurred after 5 ps, the decomposition reaction is diffusion-controlled and has a much lower reaction rate.

In the region with a locally enhanced number of OCH_2 we observed spontaneous re-formation of small oligomers in less than 1 ps. The apparent conflict between the short lifetime of dimers and the 1 eV bond energy in vacuum was resolved by determining the free-energy profile of dimerization in the liquid. The breaking of the dimer acetal bond was found to require only 10 kJ mol^{-1} and to be barrierless. Reaction free energies of this order of magnitude are in agreement with estimates deduced from the experimental thermochemistry of TXN polymerization (see ref 4 and references therein). On the basis of an analysis of the local structure of the liquid surrounding the carbocation, the drastic reduction of effective binding energy was rationalized as the result of solvation of the carbocation. Attracted by charge-induced dipole interaction, the O atoms of the carbonyl bonds of formaldehyde molecules accumulate in a (loose) coordination around the carbocation and compete with a carbonyl oxygen reacting with the carbocation. We have not been able to find experimental data for a quantitative verification of the fast time scale of the reaction kinetics observed in *ab initio* MD. We suggest, however, that factors such as solvation effects, which affected free energies and reaction rates in the small and simplified model of our simulation, are more general and also play a role in more complex systems.

Simulation of the reactive TXN mixture is an instructive illustration of the various issues that arise in *ab initio* MD applications to condensed-phase chemistry. Hence, we will conclude the discussion with a few more technical comments. A first crucial step is to define a model. On the one hand, there is a lower limit to system size, below which effects of the environment (solvent) on the reaction are no longer described properly. On the other hand, relaxation times in the system impose a minimum run length, which sets an upper limit on the number of atoms. In simulations in which the reaction coordinate (e.g., the length of the bond that is formed or broken) is the only slow variable, the time-scale problem can be circumvented by using constrained dynamics methods. However, if the relaxation of solvent degrees of freedom also exceeds MD times scales, the constrained dynamics approach is of little help. The TXN system was a fortunate example for which, given the current state of technology, a compromise between system size and run length was achieved. This enabled us to use free dynamics to obtain an unbiased picture of the dynamics of spontaneous reactive events and constrained dynamics to explore the corresponding thermochemistry. Hence, from the point of view of the statistical mechanics, the TXN simulation was an appropriate test of the *ab initio* MD approach to chemical reactions that produced encouraging results.

A more critical question concerns the accuracy of the DFT. Particularly the reaction energies discussed in the appendix give rise to concern. Protonation energies obtained by the GC functional applied here (B) are fairly accurate. However, the dimerization energy (reaction R3 in Table 5), which is the energy gained by replacing a double (carbonyl) CO bond by two single (acetal) CO bonds, is seriously underestimated. The deficit in binding energy is of such a magnitude that the error accumulated in three of these carbonyl−acetal bond exchanges

Table 2. Formaldehyde Geometry and Dipole Moment[a]

	DFT			HF	MP2	CCSD[b]	
	B	BP	B(VdB)	TZVDP	TZVDP	TZ+2P	exp
d(CO), Å	1.219	1.215	1.232	1.178	1.210	1.204	1.208[b]
d(CH), Å	1.111	1.117	1.112	1.092	1.099	1.098	1.116[b]
∠(HCH), deg	115.7	116.0	116.6	116.1	116.3	116.6	116.5[b]
μ, D			2.33		2.32		2.33[b]

[a] Reference 26. [b] Reference 27. [a] Geometric properties of a formaldehyde molecule calculated in the GC LDA (B, BP) compared to results from various computational methods and experiment (exp). Hartree−Fock (HF) and MP2 results have been obtained using the Turbomole package.[25] The data labeled B(VdB) are DFT results of a previous study of vacuum protolysis,[9] for which we used pseudopotentials generated according to the Vanderbilt (VdB) scheme, which are softer than the Trouiller−Martins pseudopotentials we apply in the present calculation.

makes the TXN molecule only marginally stable with respect to three formaldehyde molecules (reaction R4 Table 5). This reduced stability of the "acetal" bond must have accelerated the reaction dynamics in our simulation and shifted the chemical equilibrium to higher formaldehyde concentrations. Although it is unlikely that the validity of the qualitative conclusions of our work (as summarized above) is affected by these inaccuracies in the energetics, a better quantitative analysis will require a more reliable density.

A further DFT-related problem of the *ab initio* simulation of condensed systems is the uncertainty in the thermodynamic state. Temperature and volume (density) are specified in our system. The corresponding pressure, a quantity that is difficult to calculate in the *ab initio* MD approach, is unknown. Deviations from the experimental equation of state are probably not insignificant (for an investigation of the equation of state of solid formaldehyde see appendix A.3). This is a serious complication for a quantitative comparison of experimental kinetic and thermochemical data. Moreover, with regard to the accuracy of intermolecular interactions, further progress is required in the development of density functionals for molecular systems. However, we hope to have shown with the present simulation that despite these uncertainties, *ab initio* MD simulation is able to yield important insights in the chemical processes in the solution, and we are optimistic concerning the prospects of applying this technique in the future.

Appendix A. Gas-Phase Structure and Energetics

1. Molecular Structure. We summarize here select relevant gas-phase geometries and energies determined by the DFT method outlined in section III.A. We also compare these results with those obtained by different computational approaches and, if available, with experimental data. The gas-phase DFT calculations have been performed using the identical pseudopotentials and plane−wave basis set (see section III.A) as applied in the simulation of the reactive liquid. The molecules are placed in a simple cubic box of length $l = 20$ au ≈ 10.5 Å. Boundary effects are treated by the decoupling scheme mentioned in section III.B. Molecular equilibrium geometries are obtained by a quasi-Newtonian optimization method adapted from standard quantum chemistry technology.

The structure and electric dipole moment of formaldehyde are given in Table 2. Table 3 is a detailed list of structural characteristics of 1,3,5-trioxane (TXN) and the protonated derivative of this molecule. Table 4 describes the geometries of protonated formaldehyde and its dimer with formaldehyde. The DFT structures based on the B and BP functionals are compared to Hartree−Fock (HF) results and the geometries found when a correction for correlation effects in the MP2 approximation is applied. The HF and MP2 calculations have been performed using the Turbomole package[25] and the TZVDP basis set available in this code. For the sake of completeness, we have also included the results for formaldehyde and TXN from a previous publication of ours on gas-phase dynamics, which were obtained for the B functional using supersoft pseudopotentials generated according to the Vanderbilt scheme.[9]

Table 3. Trioxane and Protonated Trioxane Geometries[a]

	DFT			HF	MP2	
	B	BP	B(VdB)	TZVDP	TZVDP	exp
			$C_3H_6O_3$			
d(CO)	1.446	1.427	1.445	1.386	1.408	1.422[b]
d(CH)	1.086	1.094		1.075	1.081	
d(CH′)	1.101	1.112	1.10	1.090	1.097	
∠(COC)	109.3	108.5	109.9	111.5	108.5	110.3[b]
∠(OCO)	111.5	111.3	111.4	111.1	111.5	112.2[b]
∠(HCH)	111.4	111.6	111.5	110.2	111.2	
∠(OCOC)	57.7	58.8		55.2	58.6	
			$C_3H_6O_2O^+H$			
d(HO_h)	0.984	0.992		0.953	0.976	
d(O_hC_1)	1.639	1.594		1.508	1.539	
d(C_1O)	1.367	1.369		1.339	1.353	
d(OC_2)	1.464	1.452		1.401	1.422	
∠($H_1O_hC_1$)	107.8	108.3		111.0	108.0	
∠($C_1O_hC_1$)	105.9	106.1		110.3	107.0	
∠(O_hC_1O)	109.3	109.0		108.0	108.9	
∠(C_1OC_2)	113.6	112.2		114.0	111.5	
∠(OC_2O)	108.4	108.5		108.6	108.6	
∠($C_1O_hC_1O$)	51.8	54.6		53.0	55.2	
∠($O_hC_1OC_2$)	60.4	61.2		58.1	61.0	
∠(C_1OC_2O)	64.2	64.1		61.1	64.1	

[a] Structural characteristics of 1,3,5-trioxane ($C_3H_6O_3$) and the protonated derivative ($C_3H_6O_2O^+H$). Distances are in angstroms; bending (∠(ABC)) and torsion (∠(ABCD)) angles in degrees. The oxygen atom that binds the hydrogen is indicated by O_h. Entries C_1 and C_2 are carbons directly bonded to O_h and separated from O_h by one CO unit, respectively. [b] Reference 27.

The numbers in Tables 2−4 show the expected trend that is characteristic for the various computational methods. For the few properties for which experimental data are available, the agreement of MP2 is best with the only marginally larger discrepancies for BP. Taking the MP2 data as a reference, we notice that the B bond distances are consistently longer. For CO bond lengths, the difference is at least a few hundredths of an angstrom. The BP distances, although still longer, are closer to the MP2 results. HF, on the other hand, yields significantly shorter bond lengths than those of the MP2 data. For the bond and torsion angles the B, BP, and MP2 results are similar, whereas HF yields values that show considerable deviations from the other three sets.

Of particular interest are two CO distances that play a role in the polymerization reaction. These are also the entries in

(25) Ahlrichs, R.; Baer, M.; Haser, M.; Horn, H.; Kuelmel, M. *Chem. Phys. Lett.* **1989**, *156*, 165.
(26) Scuseria, G. E.; Schaefer, H. F., III. *J. Chem. Phys.* **1989**, *90*, 3629.
(27) *Handbook of Chemistry and Physics*, 75th ed.; Lide, D. R., Ed.; CRC Press: Boca Raton, 1994.
(28) Wolf, J. F.; Staley, R. J.; Koppel, I.; Taagepera, M.; McIver, R. T., Jr.; Beauchamp, J. L.; Taft, R. W. *J. Am. Chem. Soc.* **1977**, *99*, 5417.
(29) Fox, A.; Wlodek, S.; Hopkinson, A. C.; Lien, M. J.; Sylvain, M.; Rodriguez, C.; Bohme, D. K. *J. Chem. Phys.* **1989**, *93*, 1549.

Table 4. Protonated Formaldehyde and Dimer Geometries[a]

	DFT		HF	MP2
	B	BP	TZVDP	TZVDP
	$HOCH_2^+$			
$d(HO_h)$	0.992	0.995	0.957	0.980
$d(O_hC^+)$	1.266	1.261	1.227	1.247
$\angle(HO_hC^+)$	115.2	115.1	116.9	114.5
	$HOCH_2OCH_2^+$			
$d(HO_h)$	0.980	0.980	0.945	0.965
$d(O_hC)$	1.322	1.334	1.328	1.331
d(CO)	1.866	1.691	1.543	1.608
$d(OC^+)$	1.241	1.242	1.213	1.236
$\angle(HO_hC^+)$	112.7	112.2	113.2	111.6
$\angle(COC^+)$	120.1	118.5	122.8	118.7
$\angle(C^+OCO_h)$	14.1	7.1	14.5	11.2
$\angle(OCO_hH)$	93.1	95.6	100.7	97.3

[a] Structural characteristics of protonated formaldehyde ($HOCH_2^+$) and the acetal dimer ($HOCH_2OCH_2^+$) with formaldehyde. Distances are in angstroms; bending ($\angle$(ABC)) and torsion ($\angle$(ABCD)) angles in degrees. The oxygen atom binding the hydrogen is indicated by O_h. C^+ is the carbon atom of the terminal (cationic) methylene group.

Table 5. Protonation and Acetal Bond Energies[a]

	DFT		HF	MP2	
	B	BP	TZVDP	TZVDP	exp
R1	752(717)	740(705)	775(741)	737(703)	731,[b] 719[c]
R2	843(812)	816(785)	825(795)	807(777)	
R3	102(84)	138(119)	107(90)	130(113)	
R4	7(−43)	145(95)	119(69)	160(110)	125[d]

[a] Reaction energies in vacuum of four relevant reactions. Values given in kJ mol^{-1}. The numbers in parentheses are the zero-point corrected energies calculated from the BP frequencies for the DFT results and the scaled Hartree−Fock frequencies for the HF and MP2 results.

$$H^+ + OCH_2 \rightarrow HOCH_2^+ \quad \text{(R1)}$$

$$C_3H_6O_3 + H^+ \rightarrow C_3H_6O_2O^+H \quad \text{(R2)}$$

$$HOCH_2^+ + OCH_2 \rightarrow HOCH_2OCH_2^+ \quad \text{(R3)}$$

$$3OCH_2 \rightarrow C_3H_6O_3 \quad \text{(R4)}$$

[b] Reference 28. [c] Reference 29. [d] Calculated from thermochemical data of refs 30 and 31.

the table for which the discrepancies are most serious. The first is the length of the bond of the C_1 carbon to the hydrogenated oxygen O_h in protonated TXN (indicated by $d(O_hC_1)$ in Table 3). As we observed in our previous MD study of gas-phase protolysis, this is the bond that is the first to break after attachment of the proton. The second is the bond in the dimer (d(CO) in Table 4, see also Figure 5)) that is formed when the carbocation in protonated formaldehyde attacks the carbonyl O atom in formaldehyde. Because of their reactivity, the lengths of these bonds are the largest in the list of Tables 2−4. For B, BP, and MP2 the dimer bond exceeds 1.6 Å, the maximum value being the d(CO) = 1.864 Å value for B, which is almost certainly an overestimation. This "anomalous" length as well as the other geometric features in Table 4, namely the $\angle(COC^+)$ angle of ∼120° (in all approaches) and the short C^+O distance, rule out a standard acetatic bond. They reflect indeed the special nature of the weaker bonding in the protonated dimer, where the hybridization of the oxygen keeps an sp^2 character and favors the partial delocalization of the positive charge. Pictorially, such a bonding pattern can be described using the resonance formula

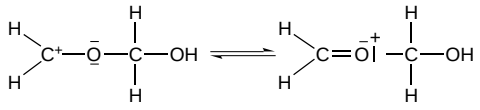

(12)

1 **2**

with larger participation of configuration **2**.

2. Proton Affinities and Formation Energies. The basic events in the reactions described in section II.A involve a proton transfer or the breaking or formation of a CO bond. The reaction energy ΔH at zero temperature of three elementary examples of these processes are listed in Table 5. Reactions R1 and R2 are the addition of a proton to formaldehyde or trioxane, respectively (first step in (3) of section II.A). Reaction R3 is the making of the CO forming a formaldehyde and protonated formaldehyde dimer (Figure 5b and (5) with n = 0). ΔH for R4 is the net energy that is released when three formaldehyde molecules are linked in a TXN ring. As in Tables 2−4 the results of the B and BP functional are again compared to energies obtained from the HF and MP2 methods.

The B, BP, and MP2 energies for reaction R1 are very similar. Despite yielding a somewhat higher ΔH value, the error of a few percent in the HF result is not excessively great. This supports the conclusion that proton affinities are not very sensitive to correlation effects. A similar trend is observed for TXN protonation (R2). Dimerization (R3), on the other hand, is a considerably less exothermic process compared to protonation. Moreover, correlation effects can be expected to be important, as is already indicated by the variation of the d(CO) bond length in Table 4. The value of ΔH of R3 in Table 5 also shows significant relative discrepancies when the data of the four computational approximations are compared. Note, however, that for all three reactions R1, R2, and R3, BP and MP2 give almost the same ΔH. The largest scattering in the computed ΔH values is found for R4. In the approximation of the B functional, trioxane is thermodynamically unstable with respect to dissociation into formaldehyde monomers. Compared to B, the ΔH for BP is almost 1 eV larger. For R4 we can obtain an experimental estimate for ΔH from low-temperature thermochemical data.[30,31] Comparing these values, we see that BP underestimates the binding by 30%. The value of ΔH for MP2 is closest to that from experiment.

A first comment that can be made on the basis of a survey of the data in Tables 2−5 is that the HF approximation is less accurate than the two DFT methods. More important for our purposes, these calculations also illustrate the differences between the two GC DFT approaches. With the GC for correlation according to Perdew (BP) included, bond lengths become shorter, proton affinities smaller, and CO bond formation energies larger. If the limited information from experiment supplemented with the results of the MP2 calculation are used as a criterion, the conclusion is that for the intramolecular properties listed in Tables 2−5 the BP functional has the most reliable overall performance.

3. Stability of the Formaldehyde Crystal. Employing the B functional in the simulation of the TXN liquid was motivated by the outcome of an evaluation of GC functionals applied to intermolecular interactions in condensed phases (solid and liquid). Whereas the high-temperature solid of formaldehyde is unstable against polymerization, it is possible to prepare by means of vapor deposition a stable molecular crystal at low temperature.[32] The unit cell is tetragonal, containing eight OCH_2 molecules arranged in four-member squares. The distance between the carbon and oxygen atoms that make up the edges

(30) Chao, J.; Wilhoit, R. C.; Hall, K. R. *Thermochim. Acta* **1992**, *200*, 41.
(31) Dorofeeva, O. V. *Thermochim. Acta* **1992**, *200*, 121.
(32) Weng, S.-X.; Torrie, B. H.; Powell, B. M. *Mol. Phys.* **1989**, *68*, 25.

of a square is 2.75 Å.[32] This is an indication that the forces that stabilize this structure are not due to chemical bonding but are of intermolecular origin. The reliability of the B and BP functionals for this system was investigated by optimizing the crystal structure for a series of different values of (fixed) cell volume. The initial configurations for the optimization were obtained by uniform scaling of the tetragonal lattice parameters. For the B functional the minimum energy structure is in good agreement with experiment. The equilibrium cell volume is only a few percent larger than that of experiment. Applying the BP functional, however, we found the molecular crystal to be chemically reactive. The squares of OCH_2 molecules contracted to form cyclic tetramers (TEXN). The equilibrium volume of these molecular crystals of TEXN is 25% smaller than the volume of the experimental OCH_2 crystal.

These results for the solid appear to contradict the data in Table 5 for the gas-phase reaction energies. A similar (although less spectacular) inconsistency was found for hydrogen bonding in water. The binding energy of the water dimer obtained using the BP functional is more accurate than the B result. However, the BP functional overestimates the strength of hydrogen bonding in liquid water and the B functional gives a better description of the structure and dynamics of the liquid.[17,18]

JA970935O